



Near-equatorial tropical cyclone formation in western North Pacific: peak season and controlling parameter

Yan Li^{1,3} · Tim Li^{1,2} · Caifang Fu¹ · Pang-Chi Hsu¹

Received: 22 July 2017 / Accepted: 31 May 2018 / Published online: 14 June 2018
© Springer-Verlag GmbH Germany, part of Springer Nature 2018

Abstract

The near-equatorial (0° – 5° N) tropical cyclones (TCs) in the western North Pacific (WNP) exhibit distinctive seasonal variability, with a peak in the boreal winter, as opposite to that in the main TC development region over the WNP. The mechanism behind such a distinctive annual evolution is investigated through the diagnosis of the genesis potential index (GPI). By isolating the effect of various environmental parameters, we found that the increase of the near-equatorial GPI in the boreal winter is primarily attributed by the low-level absolute vorticity. As the season progresses from the boreal summer to winter, the northeasterly trade wind turns anticlockwise near the equator, leading to maximum low-level cyclonic vorticity near 5° N. In addition, the mean flow advection also plays a role in “allowing” more time for perturbations to grow in the near-equatorial zone in DJFMAM than in JASO. The seasonal changes of other environmental conditions, such as relative humidity and sea surface temperature, are not as critical. While the effect of area-averaged vertical wind shear is small due to the opposite signs between western and eastern sectors of the WNP in the boreal winter, a moderate vertical shear over 140 – 160° E, 2 – 5° N may favor the development of TC-like disturbances in the region. Our analysis results suggest that dynamic parameters are more important for the formation of near-equatorial TCs.

Keywords Near-equatorial tropical cyclone · Tropical cyclone genesis · Genesis potential index

1 Introduction

Classic meteorology text books state that tropical cyclone (TC) genesis usually happens 5° away from the equator, because Earth’s planetary vorticity (i.e., Coriolis parameter) is critical for connecting rotational and convergent flow components (Gray 1968; Anthes 1982; Li et al. 2012). In reality, we have observed tropical disturbances developing

into tropical storms (17 m s^{-1}) or typhoon strength within 0° – 5° N. For example, Typhoon Sarah (1956) was intensified into typhoon strength at 4° N (Fortner 1958). Typhoon Kate (1970) formed over 140° E, 5° N on 13 October 1970, then traveled westward and reached its minimum sea level pressure at 4.5° N (Holliday and Thompson 1986). Typhoon Vamei (2001) formed at 1.5° N in the South China Sea in December 2001, and maintained the typhoon strength for 12 h (Chang et al. 2003; Chambers and Li 2007; Juneng et al. 2007). Motivated by these observations, we intend to understand the seasonal variability and environmental conditions favorable for TC formation within the near-equatorial belt of 0° – 5° N.

The WNP is the most active basin of TC genesis. The mean flow and perturbations in the WNP are quite different from those in the other basins (see Li 2012; Li and Hsu 2017 for comprehensive reviews on this topic). Most of TCs in the WNP are formed in the monsoon trough region, during an active season in the boreal summer and early fall (from July to October) and an inactive season in the boreal winter and spring (from December to May). However, as shown in previous studies (Holliday and Thompson 1986; Yi and Zhang

✉ Yan Li
yanlee@nuist.edu.cn

¹ Key Laboratory of Meteorological Disaster, Ministry of Education (KLME)/Joint International Research Laboratory of Climate and Environmental Change (ILCEC)/ Collaborative Innovation Center on Forecast and Evaluation of Meteorological Disasters (CIC-FEMD), Nanjing University of Information Science and Technology, Nanjing, China

² Department of Atmospheric Sciences, School of Ocean and Earth Science and Technology, University of Hawaii, 2525 Correa Rd., Honolulu, HI 96822, USA

³ College of Atmospheric Science, Nanjing University of Information Science and Technology, Nanjing, China

2010), near-equatorial TCs peak in winter/early spring, with more TCs happening in the boreal winter in the winter trade region. A natural question to ask is what causes such a distinctive difference in peak season between off-equatorial and near-equatorial TCs?

To answer the question, one needs to understand what the key environmental parameters controlling TC genesis in the near-equatorial region are. Previous studies suggested that favorable environmental conditions for TC genesis include sufficiently warm sea surface temperature (SST), cyclonic vorticity, conditional unstable atmospheric stratification, high relative humidity in the lower-mid troposphere, and low vertical wind shear (VWS) (e.g., Gray 1979; Emanuel 2000). However, the key genesis parameters may differ in different basins (Fu et al. 2012; Peng et al. 2012) or in different seasons. Thus, it is critical to understand the key environmental parameters that control cyclogenesis near the equator.

The objectives of the present study are to reveal the seasonal variability characteristics of the near-equatorial TCs in the WNP and to understand the cause of their distinctive seasonal variability compared to the TCs formed in the monsoon trough north of 5°N. An attention will be paid to environmental parameters that control TC genesis near the equator. The remaining of this paper is organized as follows. Data and methodology are described in Sect. 2. In Sect. 3, we show the seasonal variability of observed TCs in the near-equatorial region during 1979–2012. The relative roles of dynamic (vorticity, vertical shear) and thermodynamic (moisture, maximum potential intensity) environmental parameters in affecting TC genesis are examined in Sect. 4. In Sect. 5, we discuss the cause of opposite active seasons between TCs formed in the monsoon trough and those formed near the equator. Finally, conclusions are given in Sect. 6.

2 Data and method

2.1 Data

The best-track data from the Joint Typhoon Warning Center (JTWC) were used to determine TC genesis time and location in the WNP. In many occasions, JTWC started a TC warning when the system has a tropical depression (TD) intensity. But all TCs studied here have a final intensity exceeding the tropical storm (TS) strength (17.2 m s^{-1}). Thus what we examined here is these tropical depressions that occurred initially in the near equatorial zone ($< 5^\circ\text{N}$) but eventually developed into a TC. The near-equatorial TCs are defined as those whose genesis locations are within 5° latitude of the equator. The large-scale environmental fields were obtained from the European Centre for Medium-Range Weather Forecasts (ECMWF) interim reanalysis (ERA-I), which has a horizontal resolution

of 1.5° by 1.5° with 37 vertical pressure levels. The meteorological fields from the ERA-I include 6-hourly wind, air temperature, relative humidity, vertical pressure velocity, and geopotential height. The ERA-I has been substantially improved over the earlier reanalysis product of ERA-40 due to the use of more satellite data in the data assimilation system (Dee et al. 2011). Daily SST data are the National Oceanic and Atmospheric Administration Optimum Interpolation (NOAA-OISST) analysis (Reynolds et al. 2007), whose resolution is $\frac{1}{4}^\circ$.

2.2 TC genesis potential index

Emanuel and Nolan (2004) developed a genesis potential index (GPI) to measure the effects of large-scale dynamic and thermodynamic environmental factors on TC genesis. The GPI consists of four parameters, absolute vorticity, relative humidity, potential intensity, and vertical shear. Following Li et al. (2013), the derivative of the GPI formula was used to quantitatively assess the relative contributions of the four environmental parameters to the GPI change.

The GPI formula is written as follows,

$$\text{GPI} = \text{Term1} \times \text{Term2} \times \text{Term3} \times \text{Term4}, \quad (1)$$

$$\text{where, Term1} = |10^5 \eta|^{3/2}, \quad \text{Term2} = (1 + 0.1 V_{shear})^{-2},$$

$\text{Term3} = (H/50)^3$, and $\text{Term4} = (V_p/70)^3$, η represents absolute vorticity at 850 hPa, V_{shear} is the magnitude of VWS, which is defined as the difference of wind speed between 200 and 850 hPa, H is the relative humidity at 600 hPa, and V_p is the maximum TC potential intensity (MPI) defined by Emanuel (2000).

The change of GPI is represented by

$$\begin{aligned} \delta \text{GPI} &= t1 + t2 + t3 + t4 \\ &= \delta \text{Term1} \times \overline{\text{Term2}} \times \overline{\text{Term3}} \times \overline{\text{Term4}} \\ &\quad + \delta \text{Term2} \times \overline{\text{Term1}} \times \overline{\text{Term3}} \times \overline{\text{Term4}} \\ &\quad + \delta \text{Term3} \times \overline{\text{Term1}} \times \overline{\text{Term2}} \times \overline{\text{Term4}} \\ &\quad + \delta \text{Term4} \times \overline{\text{Term1}} \times \overline{\text{Term2}} \times \overline{\text{Term3}} \end{aligned} \quad (2)$$

where the bar denotes a time average (say, July–October mean), and δ represents the difference between two analysis periods (say, DJFMAM minus JASO). Through this diagnosis, the relative contributions of the individual terms to δGPI can be quantitatively assessed (see Li et al. 2013 for detailed derivation).

Table 1 Monthly numbers (units: TC count per month) of near-equatorial (0° – 5° N) and off-equatorial (poleward of 5° N) TCs in the western North Pacific for the period of (1) December through May (DJFMAM) and (2) July through October (JASO). The data period is from 1979 to 2012

	WNP TC inactive season DJFMAM	WNP TC peak season JASO
Off-equatorial region ($>5^{\circ}$ N)	16.7	141.8
Near-equatorial region ($<5^{\circ}$ N)	7.0	4.5

3 Seasonal variability difference between near- and off-equatorial TCs

There are an active TC season in July–October and an inactive season from December to May in the WNP. By separating the near-equatorial and off-equatorial regions, one may notice that the TC statistics in the near-equatorial region has an opposite peak season as that in the off-equatorial region; that is, an active (inactive) season in DJFMAM (JASO) (Table 1). These results are based on data analysis for the period from 1979 to 2012. The peak active season for the major TC region (poleward of 5° N) is in July–October (JASO), during which time there were 141.8 TCs per month. In contrast, in the same region during the inactive season (DJFMAM), there were only 16.7 TCs per month. The ratio was 8.5:1.0. In a sharp contrast, the active season of the near-equatorial TCs is during the boreal winter, and the inactive season is during the boreal summer. There were on average 7 TCs per month during the boreal winter and only 4.5 TCs per month in JASO. The ratio was 1.0:1.6.

Next, we examine the genesis locations for the near-equatorial TCs during the two seasons (Fig. 1). Note that most (93%) of the near-equatorial TCs were formed in a rectangular region spanning from 135° E to 180° E and from 2° N to 5° N. To explore whether or not the seasonal contrast of the near-equatorial TCs can be attributed to the seasonal difference of SST, we also plot the climatological mean SST averaged during these months in Fig. 1. It can be seen that the climatological mean SST is warmer in the near-equatorial region. The climatological mean SST of the two seasons in the rectangular box is higher than 28.5° C, which is favorable for TC genesis. However, the fact that a warmer SST during JASO is associated with less frequent near-equatorial TCs indicates that the seasonal change of the near-equatorial TC genesis is determined primarily by large-scale atmospheric conditions, rather than by local SST.

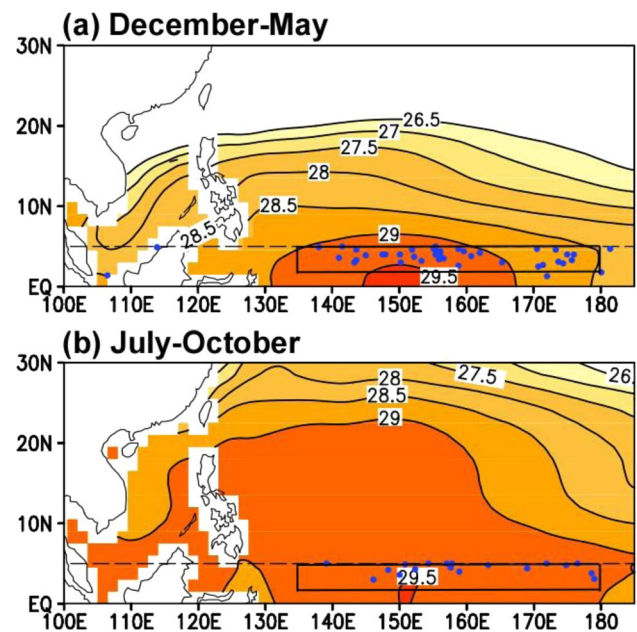


Fig. 1 Climatological mean SST ($^{\circ}$ C) and near-equatorial TC genesis locations (blue dots) during the periods of **a** December–May and **b** July–October

4 Relative contributions of environmental factors to GPI change

4.1 Relation between GPI and TC number

To examine whether the GPI is useful for describing the distinctive seasonal cycle of the near-equatorial TCs and the spatial contrast between the near-equatorial TCs and those formed over the main TC development region, we first examine the relationship between area-averaged climatological seasonal GPI averaged over the black box (135° – 180° E, 2° – 5° N) shown in Fig. 1 and the near-equatorial TC genesis number. Figure 2 shows that the area-averaged GPI represents the seasonal variability of the near-equatorial TC number well.

The spatial distributions of GPI during the two periods (December–May versus July–October) are shown in Fig. 3. The GPI reaches its maximum at 5° N in December–May, which is consistent with the occurrence of most of the near-equatorial TCs (Fig. 3a). In contrast, the maximum GPI center shifts northward in July–October, and is oriented along the monsoon trough between 10° – 20° N (Fig. 3b). Again the maximum GPI center coincides with the occurrence of major TCs in the period. Therefore, the GPI difference displayed in Fig. 3c exhibits distinctive spatial difference of TC genesis between the two periods: in December–May, major TC activity appears near and south of 5° N; and in July–October, major TC activity is located at the monsoon trough north of 10° N.

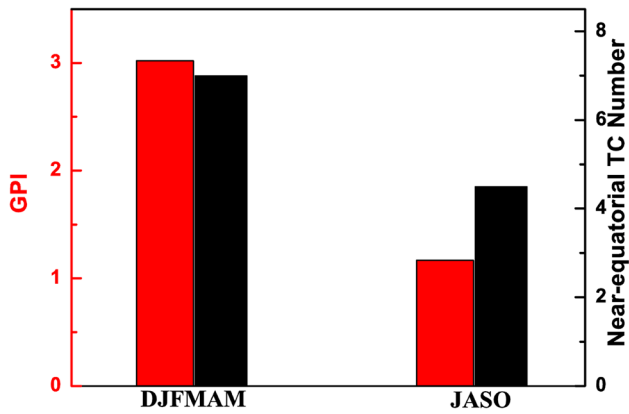
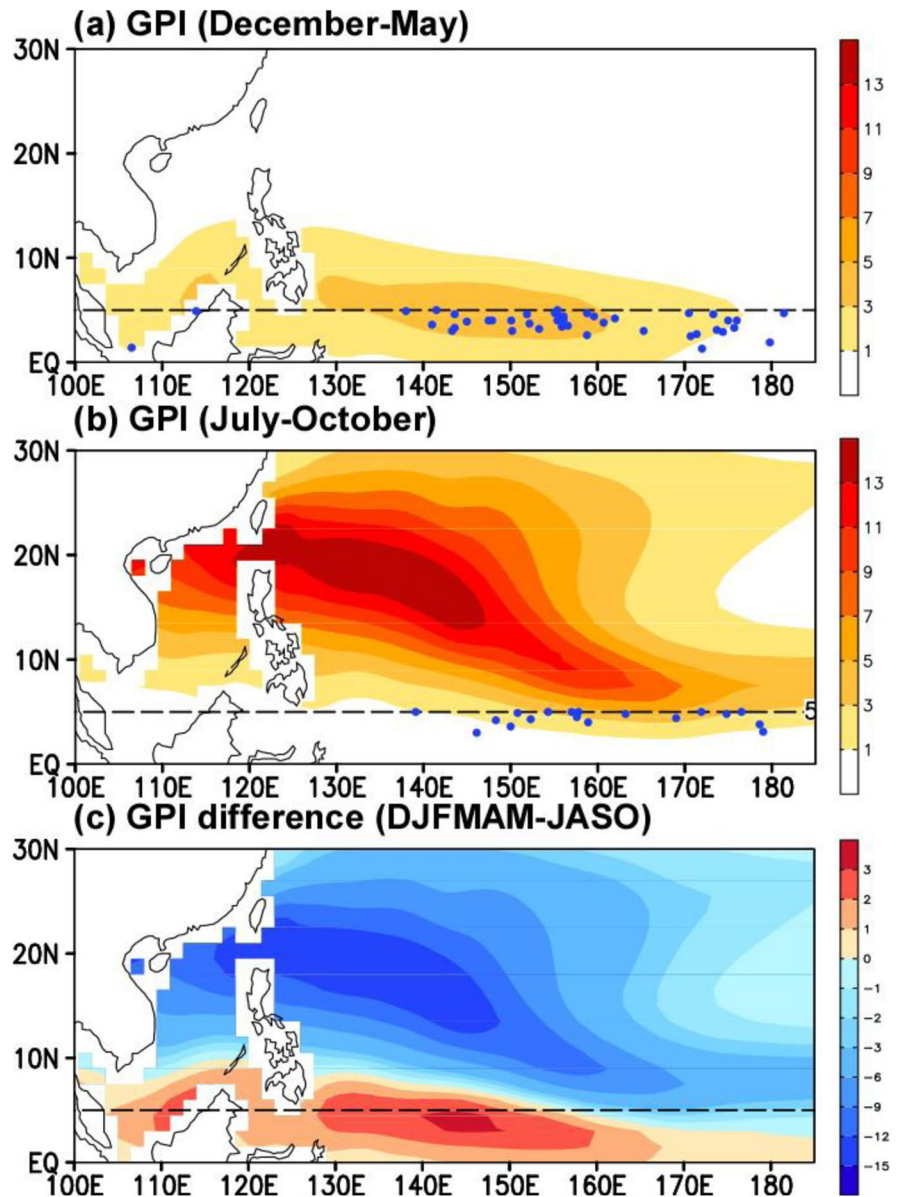


Fig. 2 Seasonal GPI (dark gray bar) averaged over 135°–180°E, 2°–5°N and near-equatorial TC number (light gray bar) in DJFMAM and JASO

Fig. 3 GPI (shading) and locations of near-equatorial TCs (blue dots) during the periods of **a** December–May and **b** July–October. **c** shows the GPI difference between the two periods (DJFMAM minus JASO)



4.2 Relative contributions of environmental factors

Given that the GPI represents the seasonal contrast of the near-equatorial TCs well, we now investigate major environmental parameters that control the seasonal difference. By applying the diagnostic Eq. (2), we intend to reveal the relative contribution of each of the four environmental parameter terms to the GPI change.

Figure 4 shows the contributions of the 850-hPa absolute vorticity term, the VWS term, the 600-hPa relative humidity term, and the MPI term to GPI difference between the two periods of December–May and July–October. The sum of the four right-hand-side terms in Eq. (2) (Fig. 4e) resembles the GPI difference pattern shown in Fig. 3c, adding the confidence to use this linear method to separate the relative contribution of each term. The diagnosis result indicates

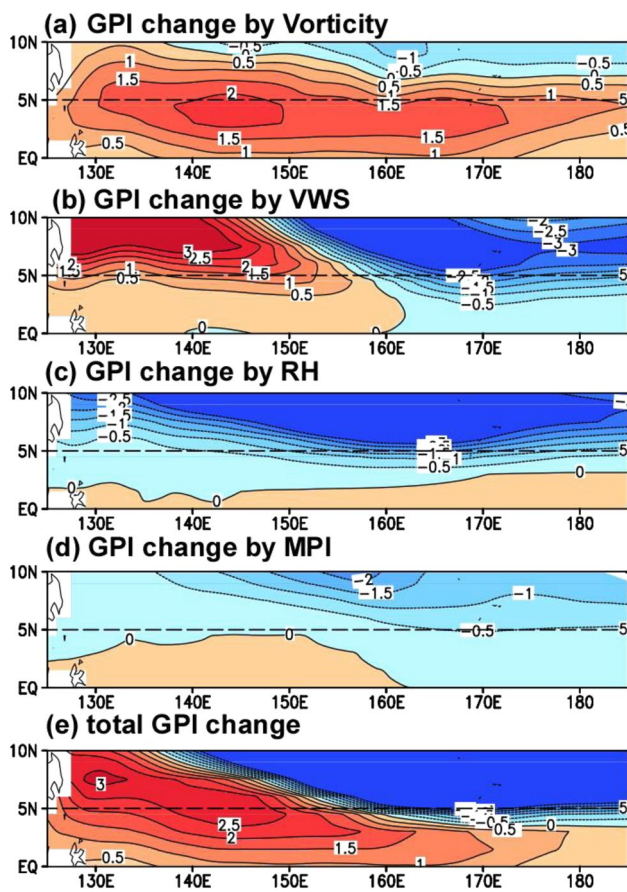


Fig. 4 Contributions of each term **a–d** on the right-hand side of Eq. (2) to the GPI change between December–May and July–October (DJFMAM minus JASO). **e** The sum of the four upper panels

that the maximum contribution to the seasonal difference of GPI in the near-equatorial region is absolute vorticity term, whose center is around 145°E. The contribution of VWS term has a dipole pattern, with a negative (positive) effect east (west) of 160°E. The relative contributions of relative humidity term and MPI term to the seasonal contrast of the near-equatorial TC formation are small.

To quantitatively measure the relative contributions of the individual terms, we calculate area-averaged GPI values and their percentage contributions to δ GPI averaged over the box of 135°E–180°, 2°–5°N. The results are shown in

Table 2. Note that the low-level absolute vorticity term plays a dominant role in contributing to the GPI change between DJFMAM and JASO. The net increase of GPI from DJFMAM to JASO is 1.63, which is primarily contributed by low-level absolute vorticity increase (contribution to GPI change: +1.91). The combined effect of VWS (contribution to GPI change: –0.12), moister effect (contribution to GPI change: –0.12), and MPI effect (contribution to GPI change: –0.06) offsets only a small portion of the vorticity effect. Therefore, the seasonal change of low-level absolute vorticity plays an important role in the increase of the near-equatorial TC frequency during DJFMAM compared to that during JASO. It is worth noting that while the area-averaged VWS effect is small, its effect appears opposite east and west of 160°E (Fig. 4b). The positive effect to δ GPI west of 160°E may help increase the frequency of near-equatorial TCs in DJFMAM than in JASO.

5 Impact of annual cycle of large-scale circulation

To reveal why the local vorticity favors more TC genesis in the near-equatorial region, we first examine the upper- and lower-tropospheric circulation patterns in DJFMAM and JASO. Figure 5 shows 200-hPa streamlines and divergence, 500-hPa vertical pressure velocity, 700-hPa relative humidity, 850-hPa streamlines and relative vorticity averaged over the two periods. The large-scale environmental fields of near-equatorial TC genesis in DJFMAM are characterized by cyclonic circulation in the lower troposphere, sufficient moisture in the mid troposphere, and divergent flow in the upper troposphere. The 850-hPa northeasterly trade wind turns anticlockwise near the equator, leading to maximum low-level cyclonic vorticity near 5°N (Fig. 5c). This cyclonic vorticity overlaps the region of strong 500-hPa ascending motion (about –0.04 Pa s⁻¹) and high 700-hPa relative humidity (greater than 60%) (Fig. 5b). The near-equatorial low-level cyclonic vorticity is accompanied by upper-level anticyclonic vorticity and divergence (Fig. 5a).

During July–October, similar environmental moisture and upper-level divergence appear in the near-equatorial region (Fig. 5d, e). For example, a center of 200-hPa divergence

Table 2 Contributions (both actual value and percentage contribution) of each term on the right-hand side of Eq. (2) to δ GPI

	t_1	t_2	t_3	t_4	Sum	δ GPI
Difference between DJFMAM and JASO	+ 1.91 (+ 117%)	– 0.12 (– 7%)	– 0.12 (– 7%)	– 0.06 (– 4%)	+ 1.61	+ 1.63

δ GPI represents the GPI change from JASO to DJFMAM, averaged over the region of 135°–180°E, 2°–5°N

t_1 denotes the GPI change caused by 850-hPa absolute vorticity, t_2 is the GPI change caused by VWS, t_3 the GPI change caused by 600-hPa relative humidity, t_4 the GPI change caused by MPI

is located south of the South Asia high (SAH) and tropical upper-tropospheric trough (TUTT). However, unlike DJFMAM, the low-level anticyclonic vorticity dominates the near-equatorial region, which is caused by the clockwise curvature of cross-equatorial flow north of the equator (Fig. 5f). Maximum cyclonic vorticity appears north of 10°N along the monsoon trough.

While the environmental conditions are important for generating tropical disturbances near the equator, the background mean flow does make a difference in terms of where the disturbances reach the tropical storm strength. While the mean flow in DJFMAM (Fig. 5c) slows down the northward movement of the near-equatorial disturbances, the mean flow in JASO (Fig. 5f) “pushes” these disturbances northward away from the equatorial zone. Such a mean flow advection effect acts as an additional mechanism to allow more frequent cyclogenesis in the near equatorial zone in DJFMAM than in JASO. This mean flow effect is backed by the observational fact that the averaged latitude to reach the tropical storm strength is 7.9°N for the near equatorial perturbations in DJFMAM but 11.2°N in JASO.

The analysis above shows that the major difference in the environmental conditions near the equator between December–May and July–October lies in the low-level vorticity field. To further illustrate the environmental condition difference between the two periods, we plot longitude–height cross sections of several key variables averaged over $2^{\circ}\text{--}5^{\circ}\text{N}$ in Fig. 6. In addition to obvious environmental vorticity difference, the atmosphere is more convectively unstable in DJFMAM compared to JASO, which can be seen from the vertical profile of equivalent potential temperature difference field (Fig. 6a). A larger value of the equivalent potential temperature in lower troposphere implies a more convectively unstable stratification, which favors TC development. In addition, the low-level convergence and mid-level ascending motion are greater in the DJFMAM period. These environmental conditions are also favorable for more frequent occurrence of the near-equatorial TCs in the boreal winter.

To understand the cause of VWS dipole contribution, we plot the VWS patterns in DJFMAM and JASO, and their relationship with the near-equatorial TC genesis in Fig. 7. The 200–850 hPa VWS with a value higher than 9 m s^{-1} is usually unfavorable for TC formation or intensification

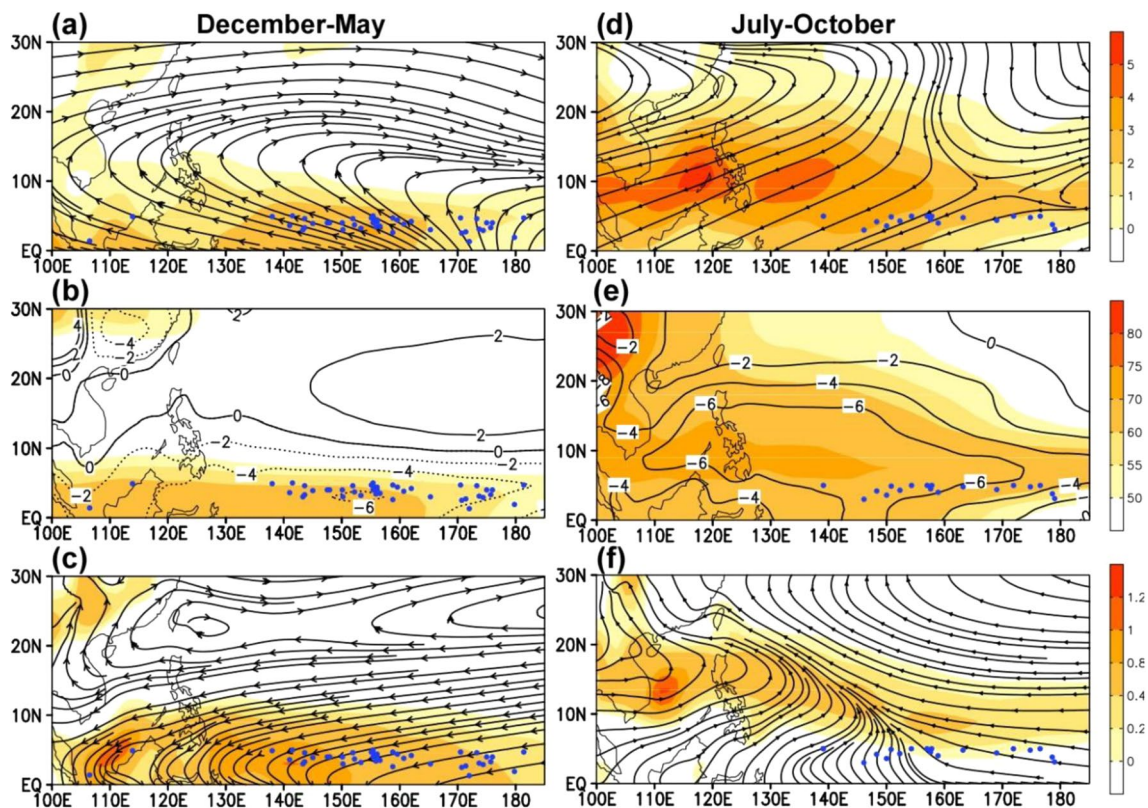


Fig. 5 **a, d** Horizontal patterns of 200-hPa streamlines and divergence (shading, 10^{-6} s^{-1}), **b, e** 500-hPa vertical pressure velocity (contour, 10^{-2} Pa s^{-1}) and 700-hPa relative humidity (shading, %), and **c, f** 850-hPa streamlines and relative vorticity (shading, 10^{-5} s^{-1})

during December–May (left) and during July–October (right). Blue dots denote the locations of near-equatorial TCs during the two periods

(e.g., DeMaria 1996; Frank and Ritchie 2001; Wong and Chan 2004). From Fig. 7a, b, one can see that almost all the near-equatorial TCs were formed in the region where the environmental VWS was smaller than 9 m s^{-1} (from 145°E to 180° and from 0° to 5°N). The average value of VWS over the formation region of the near-equatorial TCs is greater in DJFMAM than in JJASO, which is consistent with the negative role of VWS implied in Table 1. A more careful examination of regional characteristics of the VWS difference shows that a decrease (increase) of VWS appears west (east) of 160°E (Fig. 7c). As a result, the contribution by VWS to GPI change exhibits a positive (negative) effect west (east) of 160°E , as shown in Fig. 4b.

The zonal dipole pattern of the VWS difference in Fig. 7c is primarily attributed to the zonal wind component. Figure 8

shows the longitude-height cross sections of the zonal wind averaged over $2^\circ\text{--}5^\circ\text{N}$ during the two periods. In DJFMAM, the zonal wind shear is the easterly shear (westerly shear) west (east) of about 160°E (Fig. 8a). In JJASO, the easterly shear is much stronger west of 160°E due to stronger easterly in the upper troposphere and westerly in the lower level (Fig. 8b). As a result, the zonal wind shear is much weaker in DJFMAM than in JJASO west of 160°E . To the east of 160°E , there is westerly shear in DJFMAM compared to near zero shear in JJASO. The zonal wind shear characteristic is consistent with the total VWS change characteristic illustrated in Fig. 7c.

6 Conclusions and discussion

While the peak (inactive) phase of TC genesis frequency in the main development region of the WNP occurs in July–October (December–May), the near-equatorial TC genesis frequency exhibits an opposite characteristic, with a peak in December–May and an inactive phase in July–October. The cause of such a distinctive evolution characteristic is examined based on the diagnosis of TC GPI. It is found that the major cause lies in the distinctive seasonal variability of environmental low-level vorticity in the near-equatorial region. In July–October, maximum low-level vorticity appears north of 10°N and along the WNP monsoon trough, while a negative vorticity appears in the near-equatorial region. In contrast, in December–May, maximum cyclonic vorticity appears near 5°N , which is caused by the curvature of southward cross-equatorial flow. The mean flow advection also plays a role in modulating the track of the perturbation vortex, favoring more frequent TC genesis in the near-equatorial zone in DJFMAM while “pushes” the disturbances away from the near equatorial zone in JJASO. While the area-averaged VWS effect is small (contribution to GPI change: -0.12), the VWS has a positive (negative) contribution to near-equatorial TC formation in DJFMAM to the west (east) of 160°E . Compared to JJASO, the easterly shear is weaker west of 160°E and the westerly shear is stronger east of 160°E in DJFMAM. Other environmental conditions, such as SST, relative humidity and MPI, are quite similar near the equator between the two periods.

In addition to aforementioned environmental vorticity, moisture, potential intensity, and VWS effects, we note that there is a marked difference in large-scale low-level convergence, mid-level vertical motion and equivalent potential temperature vertical profile between the two periods. Greater low-level moisture and stronger mid-tropospheric ascending motion, as well as a more convectively unstable stratification, appear in December–May compared to those in July–October. These additional parameters need

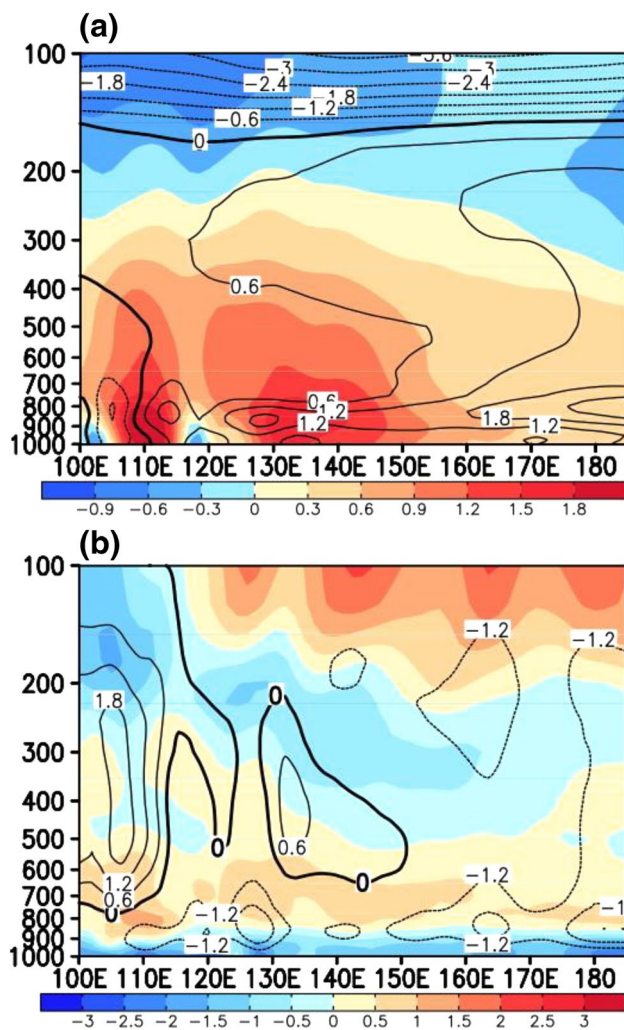


Fig. 6 Vertical-longitude cross sections of difference fields between DJFMAM and JJASO (DJFMAM minus JJASO) averaged over $2^\circ\text{--}5^\circ\text{N}$: **a** relative vorticity (shading, 10^{-5} s^{-1}) and equivalent potential temperature (contour, K); and **b** divergence (shading, 10^{-6} s^{-1}) and vertical pressure velocity (contour, $10^{-2} \text{ Pa s}^{-1}$)

to be considered in the GPI formula (Murakami and Wang 2010). Numerical model experiments need to be conducted to reveal the fundamental dynamics of TC genesis under a weak environmental vorticity condition.

Acknowledgements This study is jointly supported by the China National 973 projects (2017YFA0603802 and 2015CB453200), the NSF of China (Grants 41775058 and 41630423), NRL grant N00173-16-1-G906, NSF AGS-16-43297, Jiangsu NSF project (BK20150062), and the Priority Academic Program Development of Jiangsu Higher Education Institutions (PAPD). This is SOEST contribution number 10407, IPRC contribution number 1324 and ESMC number 219.

References

- Anthes RA (1982) Tropical cyclone: their evolution, structure and effects. *Meteorol Monogr*: 208
- Chambers CRS, Li T (2007) Simulation of formation of a near-equatorial typhoon Vamei (2001). *Meteorol Atmos Phys* 98(1):67–80
- Chang CP, Liu CH, Kuo HC (2003) Typhoon Vamei: an equatorial tropical cyclone formation. *Geophys Res Lett* 30(3):1151–1154
- Dee DP, Coauthors (2011) The ERA-Interim reanalysis: Configuration and performance of the data assimilation system. *Quart J Roy Meteor Soc* 137:553–597
- Demaria M (1996) The effect of vertical shear on tropical cyclone intensity change. *J Atmos Sci* 53:2076–2087
- Emanuel KA (2000) A statistical analysis of tropical cyclone intensity. *Mon Weather Rev* 128:1139–1152
- Emanuel KA, Nolan DS (2004) Tropical cyclone activity and global climate. In: 26th Conf. on Hurricanes and Tropical Meteorology, Miami, FL, Amer Meteor Soc, 240–241 (**Preprints**)
- Fortner LE (1958) Typhoon Sarah. 1956. *Bull Amer Meteor Soc* 39:633–639
- Frank WM, Ritchie EA (2001) Effects of vertical wind shear on the intensity and structure of numerically simulated hurricanes. *Mon Weather Rev* 129:2249–2269
- Fu B, Peng MS, Li T, Stevens DE (2012) Developing versus nondeveloping disturbances for tropical cyclone formation. Part II: Western North Pacific. *Mon Weather Rev* 140:1067–1080
- Gray WM (1968) Global view of the origin of tropical disturbances and storms. *Mon Weather Rev* 96:669–700
- Gray WM, (1979) Hurricanes: their formation, structure and likely role in the tropical circulation. *Meteorology over the tropical oceans*. James Glaiser House 155–218
- Holliday CR, Thompson AH (1986) An unusual near-equatorial typhoon. *Mon Weather Rev* 114:2674–2677
- Juneng L, Tangang FT, Reason CJC, Moten S, Hassan WAW (2007) Simulation of tropical cyclone Vamei (2001) using the PSU/NCAR MM5 model. *Meteorol Atmos Phys* 97(1):273–290
- Li T (2012) Synoptic and climatic aspects of tropical cyclogenesis in Western North Pacific. In: Oouchi K, Fudeyasu H (eds) Chapter 3. Nova Science Publishers, Inc, pp 61–94
- Li T, Hsu P-C (2017) Chapter 4 tropical cyclone formation fundamentals of tropical climate dynamics. *Springer atmospheric sciences*. https://doi.org/10.1007/978-3-319-59597-9_44
- Li T, Ge X, Peng M, Wang W (2012) Dependence of tropical cyclone intensification on the Coriolis parameter. *Trop Cyclone Res Rev* 1(2):242–253
- Li Z, Yu WD, Li T, Murty VSN, Tang G, Fredolin (2013) Bimodal character of cyclone climatology in the Bay of Bengal modulated by monsoon seasonal cycle. *J Clim* 26:1033–1046
- Murakami H, Wang B (2010) Future change of North Atlantic tropical cyclone tracks: projection by a 20-km-mesh global atmospheric model. *J Clim* 23:2699–2721
- Peng MS, Fu B, Li T, Stevens DE (2012) Developing versus nondeveloping disturbances for tropical cyclone formation. Part I: North Atlantic. *Mon Wea Rev* 140:1047–1066
- Reynolds RW, Smith TM, Liu C, Chenlton DB, Casey KS, Schlax MG (2007) Daily high-resolution-blended analyses for sea surface temperature. *J Clim* 20:5473–5496
- Wong MLM, Chan JCL (2004) Tropical cyclone intensity in vertical wind shear. *J Atmos Sci* 61:1859–1876
- Yi BQ, Zhang QH (2010) Near-equatorial typhoon development: climatology and numerical simulations. *Adv Atmos Sci* 27(5):1014–1024